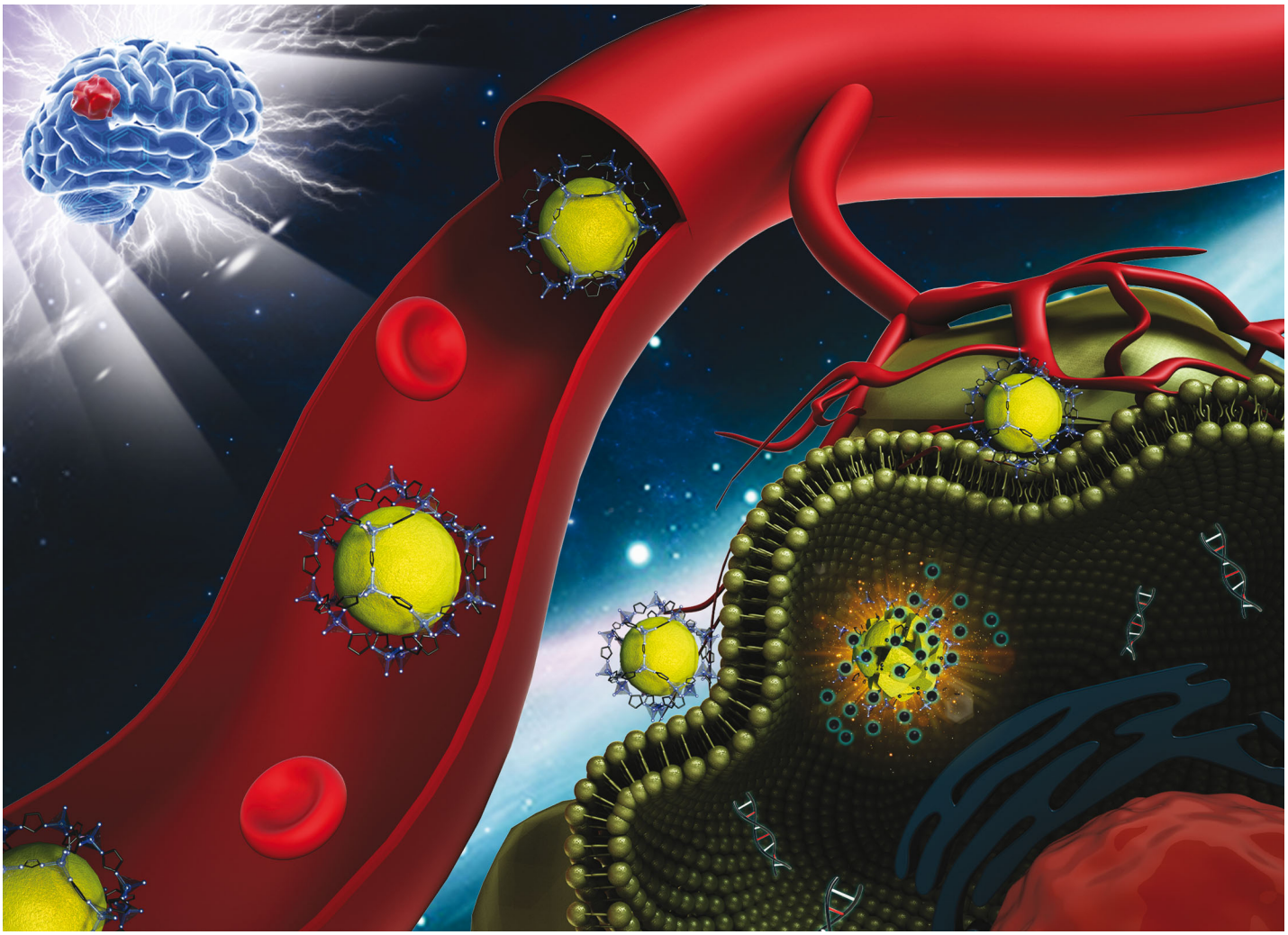

Showcasing research from the Department of Neurosurgery at the Second Affiliated Hospital of Zhejiang University School of Medicine, Hangzhou, China.

A combination of glioma *in vivo* imaging and *in vivo* drug delivery by metal–organic framework based composite nanoparticles

Metal–organic framework based composite nanoparticles (Mn-ZIF-8/5-Fu) were used for glioma treatment with high drug loading rate and pH responsive drug delivery capacity. Mn-ZIF-8/5-Fu demonstrated good magnetic resonance imaging capacity.

As featured in:

See Jianhua Wang, Anwen Shao, Jianmin Zhang *et al.*, *J. Mater. Chem. B*, 2019, **7**, 7683.

ROYAL SOCIETY OF CHEMISTRY | Celebrating IYPT 2019

rsc.li/materials-b

Registered charity number: 207890

Journal of
Materials Chemistry B

PAPER

View Article Online
View Journal | View Issue

Cite this: J. Mater. Chem. B, 2019, 7, 7683

A combination of glioma *in vivo* imaging and *in vivo* drug delivery by metal–organic framework based composite nanoparticles

Yuan-Bo Pan, †[a] Siqi Wang,†[bc] Xiuchao He,[b] Weiwei Tang,[b] Jianhua Wang,*[b] Anwen Shao*[a] and Jianmin Zhang *[a]

Received 5th August 2019,
Accepted 4th November 2019

DOI: 10.1039/c9tb01651a

rsc.li/materials-b

The success of glioma chemotherapy is hampered by low intratumoral drug concentration and severe toxicity in normal organs. Glioma diagnosis and total tumor resection depend on enhanced magnetic resonance imaging (MRI) results which provide the best solution for recognizing tumor mass anatomical details with high spatial resolution. Zeolite imidazole frameworks (ZIFs) have pore channel tunability, large specific surface area and porosity, and have broad application prospects in adsorption, catalysis and drug loading. However, there are few reports on post-synthesis ZIF-8 based multifunctional nanocomposites as a theranostic agent for *in vivo* diagnostic and therapeutic applications simultaneously. In this study, we synthesized a low toxicity bimetallic zeolitic imidazolate framework (Mn-ZIF-8) with good dispersibility and high specific surface area, which could be used for potential high drug loading. Meanwhile, we used Mn-ZIF-8 for the first time for *in vivo* MRI. T_1-weighted MR signals at tumor sites continuously increased over time after injecting Mn-ZIF-8 intravenously. Moreover, 12 hours after injecting Mn-ZIF-8 into a nude mouse bearing U87-MG tumor, a relatively high accumulation of Mn^{2+} in tumors was observed, probably due to the EPR effect of cancerous tumors. Targeted delivery significantly improves the therapeutic efficacy of Mn-ZIF-8/5-Fu in U87-MG tumor-bearing mice, resulting in 80% survival rate over 40 days of treatment. Mn-ZIF-8/5-Fu has excellent *in vivo* biocompatibility at a given dose, which induces minimal side effects on the functions of important organs. Therefore, efficient 5-Fu loaded Mn-ZIF-8 with favorable *in vivo* biocompatibility, pH responsiveness and T_1-weighted contrast MRI of tumors can be used as a promising framework for diagnostic and therapeutic applications in the case of glioma simultaneously.

Introduction

Glioma is the most common malignant primary brain tumor with high mortality and high postoperative recurrence rate.[1] Chemotherapy is an important part of glioma treatment.[2] 5-Fluorouracil (5-Fu) is an antineoplastic agent used against glioma. However, more than 80% of administered free 5-Fu is normally catabolised primarily in the liver, and as a consequence lower amounts of drug are able to reach the tumour target site.[3] Furthermore, a lack of drug efficiency is caused by a non-favourable pharmacokinetic profile (*i.e.* rapid catabolism, schedule-dependent toxicity profile, short plasma half-life (15–20 min), and poor distribution in the tumor tissue).[4] In addition, 10–20% of patients treated with standard 5-Fu show severe toxicity. Therefore, it is highly desirable to develop a simple and efficient methodology for the incorporation of 5-Fu into nanocarriers.

Zeolite imidazole frameworks (ZIFs) are a class of porous materials with a periodic three-dimensional network structure, and are generated by self-assembly and hybridization of metal ions and organic ligands.[5–7] ZIFs have pore channel tunability, large specific surface area and porosity, and have broad application prospects in adsorption, catalysis and drug loading.[8–11] On account that the ZIFs have the properties of porosity and large specific surface area, they have attracted researchers' attention in loading and releasing drugs.[7,12–14] Compared to traditional drug carriers, such as liposomes, protein nanoparticles, polymer nanoparticles, metal nanoparticles and dendrimers,[15–18] nano-ZIFs improve the bioavailability of the drug, prolong the circulation time of the drug *in vivo*, reduce the side effects caused by the high concentration of the drug,

[a] Department of Neurosurgery, Second Affiliated Hospital, School of Medicine, Zhejiang University, Hangzhou, Zhejiang, China. E-mail: zjm135@zju.edu.cn, 21118116@zju.edu.cn; Tel: +86 13805722695, +86 13867409215
[b] Department of Radiology, The Affiliated Hospital of Medical School of Ningbo University, Ningbo University School of Medicine, Ningbo, Zhejiang, China. E-mail: woxingw@sina.com; Tel: +86-574-8703-5535
[c] Department of Nuclear Medicine, Sir Run Run Shaw Hospital, Zhejiang University, Hangzhou, Zhejiang, China
† These authors contributed equally to this work.

and exhibit better targeting ability.[19–21] In addition, imidazole is a component of human amino acids, while Zn^{2+} is a trace element of the human body.[20,22] At the same time, they have excellent *in vivo* stability and pH responsiveness. When a ZIF releases drugs into the human body, its framework can also be used by the human body to minimize the toxicity to the human body. It has been reported that ZIF-8 can function as a pH-triggered carrier for 5-Fu.

Magnetic resonance imaging (MRI) is often the best technique for recognizing tumor mass anatomical details with high spatial resolution. In particular, MRI contrast agents are helpful in obtaining distinct images for glioma diagnosis. A MOF containing paramagnetic metal ions is also promising as a contrast agent for magnetic resonance (MR) imaging.[23] Compared with clinical small molecule contrast agents, the framework structure ensures that the MOF not only has a large number of paramagnetic metal centers, but also exhibits enhanced metal-based relaxation. Lin and his colleagues demonstrated for the first time the potential of a Gd-based MOF as an MR contrast agent. Their Gd-based MOF shows excellent longitudinal relaxation.[24] However, the leaching of free Gd^{3+} ions causes nephrogenic systemic necrosis, which limits its clinical application. Since Mn^{2+} and Fe^{3+} ions are also known as strong paramagnetic metal ions, their toxicity is much lower than that of Gd^{3+} ions.[25] Low toxicity manganese-based MOFs and non-toxic iron carboxylate MOFs have been developed for T_1/T_2-weighted MR contrast enhancement. A developing and attractive method to explore the application of ZIFs is to exchange the metal ions or organic ligands by post synthesis, which could keep the stability of ZIFs and explore their application. However, to the best of our knowledge, there are few reports on post-synthesis ZIF-8 based multifunctional nanocomposites as a theranostic agent for *in vivo* diagnostic and therapeutic applications simultaneously.

In this work, the proposed design combines glioma imaging and chemotherapy in a ZIF-8 matrix to construct a multifunctional theranostic nanomedical platform, which can not only diagnose glioma and visualize nanoparticle (NP) accumulation by imaging but also simultaneously deliver drugs to facilitate glioma treatment. Inspired by these, Mn-ZIF-8/5-Fu NPs were designed to combine MR imaging, ultrahigh anti-glioma drug loading and pH-responsive drug release in a single system. Furthermore, *in vitro* and *in vivo* biocompatibility, *in vivo* imaging and *in vitro* and *in vivo* tumor inhibition efficacy of the synthesized Mn-ZIF-8/5-Fu NPs were investigated in detail (Scheme 1).

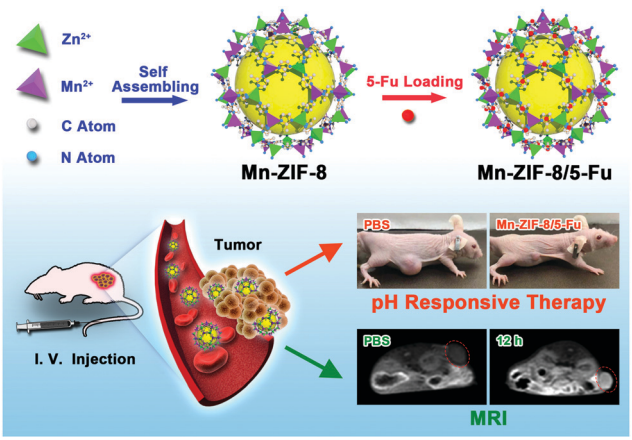

Scheme 1 Schematic illustration of the synthetic procedure for Mn-ZIF-8/5-Fu, and their application in targeted therapy and MR imaging for glioma.

Materials and methods

Reagents

5-Fluorouracil (5-Fu), dimethyl sulfoxide (DMSO) and 3-(4,5-dimethylthiazol-2-yl)-2,5-diphenyltetrazolium bromide (MTT) were purchased from Aladdin Industrial Inc. (Shanghai, China). DMEM, fetal bovine serum (FBS) and 0.25% Trypsin-EDTA were purchased from Gibco (Grand Island, USA). All materials for synthesis of Mn-ZIF-8 were purchased from Aladdin Industrial Inc. (Shanghai, China) and these materials were not purified prior to use. The U87-MG cell line was purchased from the Cell Bank of the Chinese Academy of Sciences (Shanghai, China).

Synthesis of Mn-ZIF-8

Generally, the synthesis of zeolite imidazole framework-8 nanoparticles is based on fast room temperature colloidal chemistry, using 6-hydrated zinc nitrate, 2-methylimidazole and methanol with a mass ratio of 1 : 2.5 : 100. The mixture was stirred for 18 hours and washed with fresh methanol and ethanol by centrifugation. The product was eventually dried at 150 °C and activated in vacuum for further use. Then 0.9 g manganese acetate was dissolved in 30 mL of methanol, and 0.3 g of ZIF-8 was dispersed in the above solution. The mixture was incubated in a preheated oven at 60 °C for 48 hours. The precipitate (expressed as Mn-ZIF-8) was centrifuged and washed several times with methanol until the supernatant became colorless. Then, the nanoparticles were immersed in methanol at 60 °C for 3 days, and the solution was replaced by new methanol (20 mL) every 24 hours. After soaking for 3 days, the sediments were centrifuged and dried in a vacuum oven. Powder X-ray diffraction (XRD) patterns were recorded on a D8 Focus diffractometer (Bruker) under Cu Kα radiation (λ = 1.54056 Å), operating at 40 kV and 40 mA. The sample was scanned in the range from 5 to 50° in step scan mode.

Preparation and release test of Mn-ZIF-8 with encapsulated 5-Fu

Mn-ZIF-8/5-Fu was prepared by immersing 5-Fu solution in a Mn-ZIF-8 suspension at a mass ratio of 3 : 1.[12] After stirring for 3 days, the mixture was recovered and washed by ultrafiltration. *In vitro* release was assessed by dialysis methods in different media including PBS (pH = 5.5) and neutral PBS containing 10% FBS.

Cytotoxicity assay

U87-MG cells were seeded in 96-well culture plates (10 000 cells per well) at 37 °C, 5% CO_2 for 24 hours. The medium was replaced with free 5-Fu, Mn-ZIF-8/5-Fu in the 5-Fu concentration range of

0.3–10 μg mL^{-1} or relatively Mn-ZIF-8 (1.2–40 μg mL^{-1}) at 37 °C. After 24 h, each well was replenished with fresh medium with 1% MTT (0.5 mg mL^{-1}) followed by incubation at 37 °C in the dark for 4 h. After that, the medium was replaced by 200 μL DMSO. The measurement was conducted using an automated plate reader (iMark (169-1130), Biorad, U.S.) at 550 nm.

Establishment of U87-MG glioma xenografts

All animal procedures were performed in accordance with the Guidelines for Care and Use of Laboratory Animals of the Zhejiang University and approved by the Animal Ethics Committee of the Zhejiang University. Male Balb/c nude mice (18–20 g, 4–6 weeks old) were purchased from Jiesijie Experimental Animal Company (Shanghai, China). The tumor model of human glioma was established by subcutaneous injection of U87-MG cells. Briefly, U87-MG cells (1×10^7 cells for one mouse) suspended in 100 μL of serum free PBS were inoculated subcutaneously in the back of Balb/c nude mice. Tumor volume = $a \times b^2/2$ (a = tumor length, b = tumor width).

In vivo MRI and biodistribution of Mn

To investigate the MRI performance *in vivo*, the U87-MG tumor bearing nude mice were divided into two groups and first anesthetized by intraperitoneal injection of chloral hydrate solution (5 wt%), and then the tumor bearing nude mice were intravenously injected with 100 μL of PBS or Mn-ZIF-8 (30 mg kg^{-1}). Then the T_1-weighted images were acquired and analyzed on a 3.0 T clinical MRI scanner (Signa HDxt, GE Healthcare, Milwaukee, WI, USA) equipped with a special animal imaging coil at room temperature. The T_1-weighted MR signal intensities were acquired from MR images *via* manually drawn regions of interest. For *in vivo* biodistribution of Mn, three U87-MG tumor bearing nude mice were administered intravenously with 100 μL of Mn-ZIF-8 (30 mg kg^{-1}) solution. After 12 h, all the tumor bearing mice were sacrificed and the distribution of Mn in vital organs, including the liver, heart, spleen, kidneys, lungs and tumor, was determined by ICP-AES analysis. For ICP-AES analysis, after these organs were freeze-dried and weighed, the sample was dissolved in 10 mL of aqua regia and reacted in an oven at 180 °C for 4 hours. The reaction solution was then made up to 50 mL and tested. The concentration of Mn in these organs was then quantified. In addition, in order to study the metabolism of Mn-ZIF-8 in healthy Balb/c mice, 100 μL of Mn-ZIF-8 (30 mg kg^{-1}) solution was injected into each mouse and executed on day 1, 7 and 14 (3 mice in each group). The main organs were removed and their Mn concentration was measured by ICP-AES.

In vivo antitumor effect of Mn-ZIF-8/5-Fu

When the tumors grew to 40–60 mm^2, 15 tumor bearing mice were divided into 3 groups (5 in each group). These mice were treated with PBS, 5-Fu and Mn-ZIF-8/5-Fu (100 μL, 8 mg kg^{-1} for 5-Fu) by tail vein injection. The mice were treated on 0, 2, 4 and 6 days. Tumor volume and body weight were measured at 2-day intervals for the whole process of treatment. After treatment, the survival time and percentage of mice were observed for 40 days. In addition, the vital organs and tumors were stained with Hematoxylin and Eosin (H&E) and examined using an optical microscope (DMI3000, Leica, Germany).

Statistical analysis

GraphPad Prism (version 6.0, GraphPad Software, San Diego, CA, USA) was used for statistical analysis. The results are presented as mean ± SD. Statistical differences were determined by Student's t test for two-group comparisons or ANOVA followed by Tukey's test for multiple comparisons among more than two groups. P-Value < 0.05 was considered statistically significant.

Results and discussion

Synthesis and characterization of Mn-ZIF-8

Due to the instability of the Mn^{2+}-4N tetrahedral geometry, there are some difficulties in incorporating Mn^{2+} into ZIF-8. Our experiments showed that the direct reaction of Mn^{2+} with 2-methylimidazole in different solvents will result in the formation of complex molecules rather than crystal structures.[26] In the Satoshi Horike group, cubic [Mn (2-methylimidazole) 2] (expressed as Mn-ZIF) was synthesized from [Mn (BH_4) 2.3THF] $NaBH_4$ in an Ar atmosphere.[27] However, the highly stable structure of Mn-ZIF hinders its further application. Recently, Cohen's team reported that the synthesized metal ions and ligand exchange in the zeolite imidazolium framework, which inspired us to introduce Mn^{2+} ions into the framework for further biomedical applications.[26] ZIF-8 was used as a precursor and the PSE method was performed according to a modified procedure. After being incubated with Mn(acac) 2 at 60 °C for 2 days, the nanoparticles (NP) turned brown. In order to remove unreacted Mn(acac) 2, it was further cultured for several days in pure methanol. In the final product, the ratio of Mn^{2+} to Zn^{2+} is 1 : 7. The scanning electron microscopy (SEM) and transmission electron microscopy (TEM) images of Mn-ZIF-8 are shown in Fig. 1a and b.[28] The size is about 80 nm, and the original crystal shape remains unchanged. The results of infrared spectroscopy also showed that the chemical structure of the product was consistent with the Brunauer–Emmett–Teller (BET) surface area of Mn-ZIF-8NPs reported previously, which was 1951.01 $m^2\ g^{-1}$ (Fig. 1c and d).[26] The crystal structure of Mn-ZIF-8 is similar to that of ZIF-8, indicating that no crystal form change occurs during the synthesis (Fig. 2c).[26] It showed that the high specific surface area of Mn-Zn-ZIF could be used for potential high drug loading. The size of Mn-ZIF-8 in the cell culture medium was about 110 nm, and the zeta potential was 30.2 mV (Fig. 1e and f). In summary, the above results together with the related literature confirm the successful preparation of the bimetallic zeolitic imidazolate framework.[26]

Drug loading/release of Mn-ZIF-8

Drug loading efficiency mainly depends on the stirring time and the ratio of 5-Fu to ZIF. The stirring time is taken as 3 days due to the fact that the drug load does not increase any more after this time, which indicates that the carrier has been

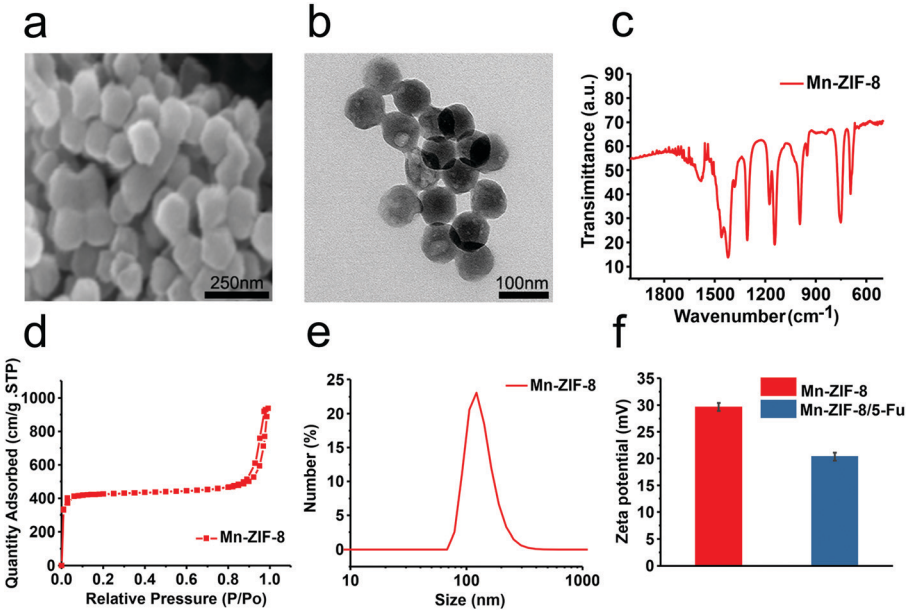

Fig. 1 Physicochemical property characterization of Mn-ZIF-8 nanoparticles: (a) SEM, (b) TEM, (c) FT-IR, and (d) BET adsorption and desorption of Mn-ZIF-8. (e) DLS of Mn-ZIF-8 in cell culture medium. (f) Zeta potential of Mn-ZIF-8 and Mn-ZIF-8/5-Fu in PBS solution.

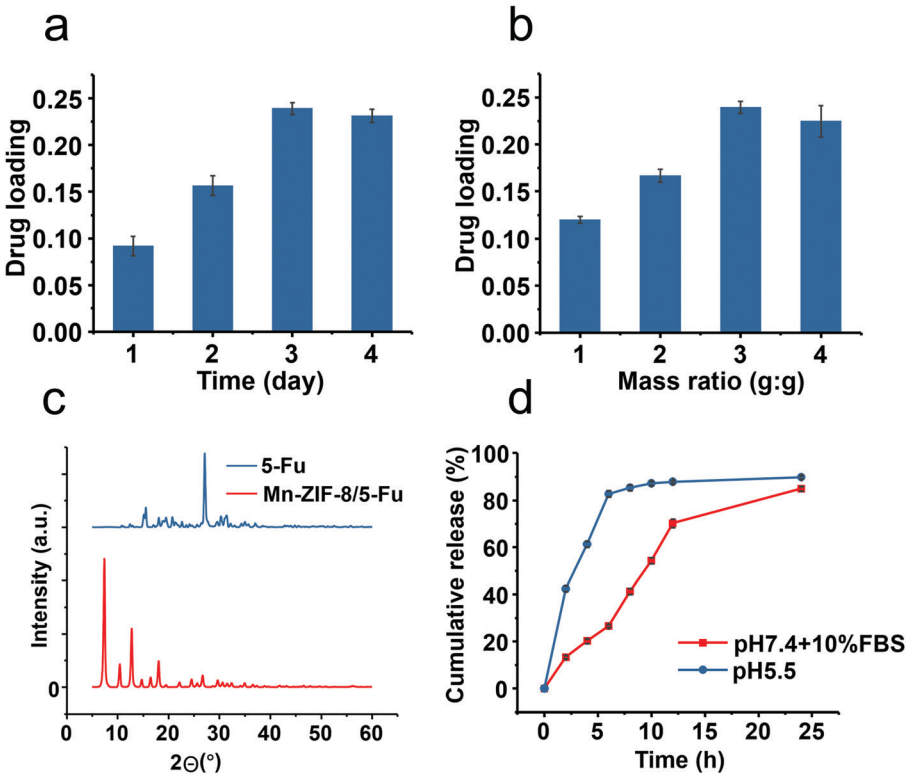

Fig. 2 5-Fu loading and characterization of Mn-ZIF-8/5-Fu. The relationship between drug loading and time (a) or concentration (b) of Mn-ZIF-8; (c) XRD of Mn-ZIF-8/5-Fu and 5-Fu; (d) *in vitro* cumulative release of 5-Fu from Mn-ZIF-8/5-Fu in PBS at pH 5.5 and pH 7.4 with 10% FBS. Data represent mean ± SD (n = 3).

saturated (Fig. 2a). The mass ratio is adjusted to 1 : 1 to obtain the maximum load, which is higher than other types of drug delivery system (DDS) (Fig. 2b). The powder XRD (PXRD) spectrum of the drug-loaded Mn-ZIF-8 did not have a diffraction peak assigned to 5-Fu, indicating that the drug may be present in the framework of the molecule or in an amorphous state (Fig. 2c). Interestingly, the nature of the solvent had little effect on the final drug loading efficiency, which may be due to the good dispersibility of Mn-ZIF-8.

The *in vitro* release profile of 5-Fu in different media is shown (Fig. 2d). Slow and sustained release was achieved in neutral environments, with less than 70% of the total released at the end of 24 hours. This release helps prevent leakage before reaching the target. Here, the initial burst in the first few hours may be due to the small proportion of payloads attached to the surface of the carrier. In contrast, when 10% fetal calf serum (FBS) was added, a relatively rapid release was observed, which revealed a possible interaction between the vector and serum proteins. In addition, a faster release of ≈80% was observed during the first 4 hours when the pH was changed to 5.5. In view of the rapid dissociation of ZIF under acidic conditions, it is obvious that drug release is closely related to the degradation of Mn-ZIF-8.

Imaging, distribution and metabolism of Mn-ZIF-8 *in vivo*

Because of the five mismatched 3D electrons of Mn^{2+}, Mn-based nanoparticles can be used as effective T_1 contrast agents in MRI. When Mn-ZIF-8 was injected intravenously into the tumor-bearing mice, enhanced T_1-weighted MR signals could be observed at the tumor site compared with the PBS group. The signal intensity of Mn-ZIF-8 increased continuously after intravenous injection and peaked at 12 hours, but the signal intensity decreased slightly at 24 hours, which indicates the cumulative accumulation process of Mn-ZIF-8 (Fig. 3a and b).

We further studied the biological distribution of Mn-ZIF-8 nanoparticles after intravenous injection. The amount of Mn^{2+} ions was measured after the tumor-bearing mice were injected with Mn-ZIF-8. At the 12th hour, a relatively high accumulation of tumors, 3.47% ID per g, was observed, probably due to the EPR effect of cancerous tumors. At the same time, although these nanoparticles also showed high levels of accumulation in the reticular endothelial system (RES), such as the liver and spleen, the Mn^{2+} levels retained in all major organs of mice decreased rapidly over time, indicating that Mn-ZIF-8 was effectively scavenged *in vivo* (Fig. 3d). Therefore, in the complex *in vivo* environment, our Mn-ZIF-8 nanostructures may gradually decompose into small molecules and ions, and then can be effectively removed from mice in a relatively rapid manner. In order to minimize the long-term toxicity of nanoparticles,

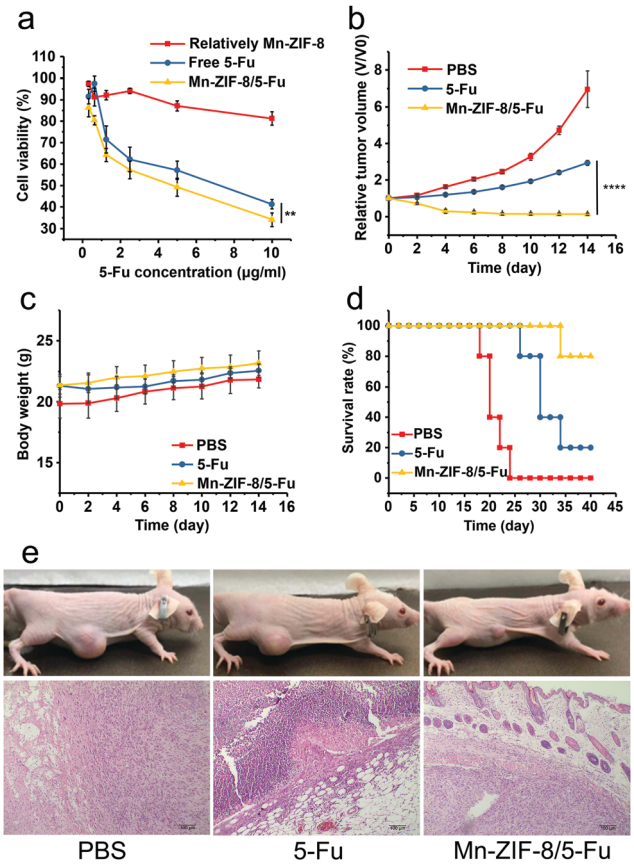

Fig. 4 Antitumor studies of Mn-ZIF-8/5-Fu in U87-MG tumor bearing mice. (a) Cytotoxicity of Mn-ZIF-8/5-Fu and 5-Fu *in vitro*; (b–d) tumor volume (b), mice body weight (c) and survival rate (d) of mice injected with PBS, 5-Fu and Mn-ZIF-8/5-Fu, (e) H&E staining sections of tumor tissues 14 days after treatment. Data represent mean ± SD (n = 5) (scale bar = 100 μm).

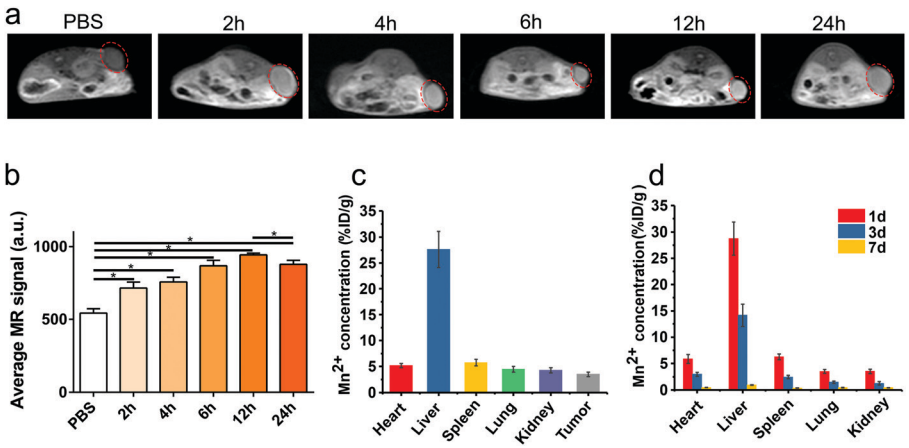

Fig. 3 Imaging, biodistribution and metabolism of Mn-ZIF-8 *in vivo*. (a and b) T_1 imaging (a) and signal statistics (b) of Mn-ZIF-8 in mice within 24 hours of injection of Mn-ZIF-8. (c) Biodistribution of Mn in tumor-bearing mice after 12 hours of injection of Mn-ZIF-8. (d) Content of Mn in healthy mice within 14 days of injection of Mn-ZIF-8. Data represent mean ± SD (n = 3).

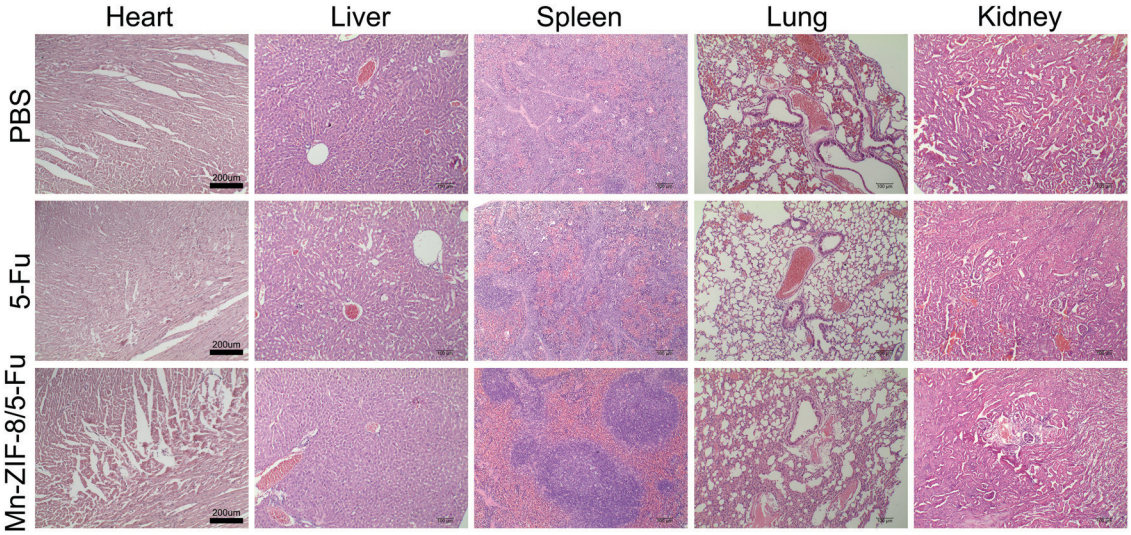

Fig. 5 H&E staining of vital organs after tail vein injection of PBS, free 5-Fu and Mn-ZIF-8/5-Fu (scale bar = 200 μm).

this nanoparticle should be preferentially selected, compared to other inorganic solid nanoparticles (such as metal, metal oxide, and metal sulfide nanoparticles) for which such an effective body removal is difficult to achieve.

In vivo anti-glioma effect of Mn-ZIF-8/5-Fu

U87-MG was used to study the anti-tumor effect of Mn-ZIF-8/5-Fu and free 5-Fu *in vitro*. Both drugs inhibited cell proliferation in a dose-dependent manner, and Mn-ZIF-8/5-Fu showed a stronger effect than free 5-Fu (Fig. 4a). Similar trends were observed in apoptotic assay, and the percentage of apoptotic cells in Mn-ZIF-8/5-Fu, 5-Fu solution and blank Mn-ZIF-8 groups was 21.33%, 3.81% and 3.52%, respectively. The increase of anti-tumor efficiency may be related to the increased drug uptake by Mn-ZIF-8.

The anti-tumor effects of different groups were tested *in vivo* after four times of drug application. The tumor size was monitored for 14 days in the treatment group. Excitingly, the growth of the tumors was slow and the tumors gradually decreased during the administration of Mn-ZIF-8/5-Fu, and no further enlargement occurred within 14 days (Fig. 4b). At the same time, the tumors of the other two groups grew rapidly during the observation period (Fig. 4b). In addition, no significant weight loss could be monitored 14 days after treatment with Mn-ZIF-8/5-Fu (Fig. 4c). It is noteworthy that all mice treated with Mn-ZIF-8/5-Fu did not relapse significantly, which resulted in 80% survival rate over 40 days of treatment, while the average life span of PBS and 5-Fu was 22 days and 30 days respectively (Fig. 4d). The H&E staining image (Fig. 4e) showed that there were vacuoles in the Mn-ZIF-8/5-Fu group compared with other groups. These excellent therapeutic effects and prolonged survival time may be due to the longer blood circulation time and the higher concentration of drug in blood, resulting in higher drug concentration in tumors.

H&E staining of important organs (heart, liver, spleen, lung and kidney) was performed to further confirm the safety of the frameworks *in vivo* (Fig. 5). After being treated with PBS and Mn-ZIF-8/5-Fu, no significant abnormalities of important organs were observed in the histopathological examination. However, the evaluation of the free 5-Fu injection group showed some damage to important organs, and descriptions in detail are as follows: (1) myocardial sarcoplasmic lysis; (2) renal inflammatory cell infiltration; (3) edema degeneration and necrosis of hepatocytes; (4) alveolar membrane thickening, capillary congestion, exudation of red blood cells and inflammatory cells in the lung; and (5) spleen atrophy and fibrous tissue proliferation. These results suggest that free 5-Fu may cause serious side effects on important organs, such as the spleen, and the framework can effectively reduce the side effects of 5-Fu on mice. Mn-ZIF-8 showed low toxicity with high drug loading and efficient antitumor efficacy with excellent MRI performance *in vivo*, which can be a potential candidate to become an effective nanoplatform in cancer precision medicine.

Conclusion

In summary, we successfully synthesized a low toxicity bimetallic zeolitic imidazolate framework (Mn-ZIF-8) with good dispersibility and high specific surface area, which could be used for potential high drug loading. The size of Mn-ZIF-8 in the cell culture medium was about 110 nm, and the zeta potential was 30.2 mV. Mn-ZIF-8 nanostructures can gradually decompose into small molecules and ions *in vivo*, and then can be effectively removed from mice in a relatively rapid manner, which minimizes the long-term toxicity on vital organs. In addition, we loaded 5-Fu on Mn-ZIF-8 to prepare Mn-ZIF-8/5-Fu. With pH responsiveness, Mn-ZIF-8/5-Fu provided a decreased premature drug release at the physiological pH level but promoted a more effective and faster drug release in the tumor cells. The pH responsive delivery significantly improved the therapeutic efficacy of Mn-ZIF-8/5-Fu and significantly prolonged the survival of U87-MG tumor bearing mice. Meanwhile, the pH

responsiveness enhanced the accumulation of Mn^{2+} in tumor sites, generating excellent T_1-weighted MR signals *in vivo*. Taken together, our study showed that the Mn-ZIF-8/5-Fu with favorable biocompatibility and pH responsiveness can be used as a novel framework for diagnostic and therapeutic applications in the case of glioma simultaneously.

Conflicts of interest

There are no conflicts to declare.

Acknowledgements

This work was supported by the National Natural Science Foundation of China (81701144 and 81371433), the China Postdoctoral Science Foundation (2017M612010), the Scientific Research Foundation of the National Health Commission – Major Science and Technology Project of Medicine and Health of Zhejiang Province (No. WKJ-ZJ-1912), and the Natural Science Foundation of Ningbo (No. 2018A610234 and 2017A610146). We thank Liyun Ge from Molecular Pharmacology Research Center, School of Pharmaceutical Science, Wenzhou Medical University, for her help with synthesis and characterization of Mn-ZIF-8. We also thank Shi-Yue Chen from Shanghai Changhai hospital for his help with MR imaging.

References

1 Q. T. Ostrom, L. Bauchet, F. G. Davis, I. Deltour, J. L. Fisher, C. E. Langer, M. Pekmezci, J. A. Schwartzbaum, M. C. Turner, K. M. Walsh, M. R. Wrensch and J. S. Barnholtz-Sloan, *Neuro-Oncology*, 2014, **16**, 896–913.
2 S. Sathornsumetee, D. A. Reardon, A. Desjardins, J. A. Quinn, J. J. Vredenburgh and J. N. Rich, *Cancer*, 2007, **110**, 13–24.
3 D. B. Longley, D. P. Harkin and P. G. Johnston, *Nat. Rev. Cancer*, 2003, **3**, 330–338.
4 O. V. Neto, S. Raymundo, M. A. Franzoi, A. do Carmo Artmann, M. Tegner, V. V. Muller, R. Z. Hahn, G. V. Alves, G. Schwartsmann, R. Linden and M. V. Antunes, *Clin. Biochem.*, 2018, **56**, 18–25.
5 J. Della Rocca, D. Liu and W. Lin, *Acc. Chem. Res.*, 2011, **44**, 957–968.
6 P. Horcajada, R. Gref, T. Baati, P. K. Allan, G. Maurin, P. Couvreur, G. Férey, R. E. Morris and C. Serre, *Chem. Rev.*, 2012, **112**, 1232–1268.
7 P. Horcajada, C. Serre, G. Maurin, N. A. Ramsahye, F. Balas, M. Vallet-Regí, M. Sebban, F. Taulelle and G. Férey, *J. Am. Chem. Soc.*, 2008, **130**, 6774–6780.
8 A. Huang, W. Dou and J. Caro, *J. Am. Chem. Soc.*, 2010, **132**, 15562–15564.
9 A. Phan, C. J. Doonan, F. J. Uribe-Romo, C. B. Knobler, M. O'Keeffe and O. M. Yaghi, *Acc. Chem. Res.*, 2010, **43**, 58–67.
10 I. Abánades Lázaro, S. Haddad, S. Sacca, C. Orellana-Tavra, D. Fairen-Jimenez and R. S. Forgan, *Chem*, 2017, **2**, 561–578.
11 Z. Jiang, B. Yuan, N. Qiu, Y. Wang, L. Sun, Z. Wei, Y. Li, J. Zheng, Y. Jin, Y. Li, S. Du, J. Li and A. Wu, *Nano-Micro Lett.*, 2019, **11**, 61.
12 S. Li, K. Wang, Y. Shi, Y. Cui, B. Chen, B. He, W. Dai, H. Zhang, X. Wang, C. Zhong, H. Wu, Q. Yang and Q. Zhang, *Adv. Funct. Mater.*, 2016, **26**, 2715–2727.
13 X. Chen, R. Tong, Z. Shi, B. Yang, H. Liu, S. Ding, X. Wang, Q. Lei, J. Wu and W. Fang, *ACS Appl. Mater. Interfaces*, 2018, **10**, 2328–2337.
14 C. G. Jones, V. Stavila, M. A. Conroy, P. Feng, B. V. Slaughter, C. E. Ashley and M. D. Allendorf, *ACS Appl. Mater. Interfaces*, 2016, **8**, 7623–7630.
15 D. J. Lundy, K.-J. Lee, I.-C. Peng, C.-H. Hsu, J.-H. Lin, K.-H. Chen, Y.-W. Tien and P. C. H. Hsieh, *ACS Nano*, 2019, **13**, 97–113.
16 X. Huang, W. Zhang, G. Guan, G. Song, R. Zou and J. Hu, *Acc. Chem. Res.*, 2017, **50**, 2529–2538.
17 X. Tian, X. Zhu, T. Yan, C. Yu, C. Shen, Y. Hu, J. Hong, H. Chen and J. Y. Fang, *Mol. Oncol.*, 2017, **11**, 1544–1560.
18 Z. Jiang, Y. Tian, D. Shan, Y. Wang, E. Gerhard, J. Xia, R. Huang, Y. He, A. Li, J. Tang, H. Ruan, Y. Li, J. Li, J. Yang and A. Wu, *Biomaterials*, 2018, **170**, 70–81.
19 J. Liu, Y. Yang, W. Zhu, X. Yi, Z. Dong, X. Xu, M. Chen, K. Yang, G. Lu, L. Jiang and Z. Liu, *Biomaterials*, 2016, **97**, 1–9.
20 Q. Wu, M. Niu, X. Chen, L. Tan, C. Fu, X. Ren, J. Ren, L. Li, K. Xu, H. Zhong and X. Meng, *Biomaterials*, 2018, **162**, 132–143.
21 T. Baati, L. Njim, F. Neffati, A. Kerkeni, M. Bouttemi, R. Gref, M. F. Najjar, A. Zakhama, P. Couvreur, C. Serre and P. Horcajada, *Chem. Sci.*, 2013, **4**, 1597–1607.
22 Z. Jiang, Y. Wang, L. Sun, B. Yuan, Y. Tian, L. Xiang, Y. Li, Y. Li, J. Li and A. Wu, *Biomaterials*, 2019, **197**, 41–50.
23 W. Wang, Z. Zhao, F. Yang, H. Wang, F. Wu, T. Liang, X. Yan, J. Li, Q. Lan, J. Wang and J. Zhao, *J. Neuro-Oncol.*, 2018, **136**, 263–271.
24 W. J. Rieter, K. M. L. Taylor, H. An, W. Lin and W. Lin, *J. Am. Chem. Soc.*, 2006, **128**, 9024–9025.
25 D. Ni, W. Bu, E. B. Ehlerding, W. Cai and J. Shi, *Chem. Soc. Rev.*, 2017, **46**, 7438–7468.
26 H. Fei, J. F. Cahill, K. A. Prather and S. M. Cohen, *Inorg. Chem.*, 2013, **52**, 4011–4016.
27 K. Kadota, E. Sivaniah, S. Bureekaew, S. Kitagawa and S. Horike, *Inorg. Chem.*, 2017, **56**, 8744–8747.
28 H. Zheng, Y. Zhang, L. Liu, W. Wan, P. Guo, A. M. Nyström and X. Zou, *J. Am. Chem. Soc.*, 2016, **138**, 962–968.